Supporting Information

Enhanced photoelectrochemical water oxidation on bismuth vanadate by electrodeposition of amorphous titanium dioxide

David Eisenberg, Hyun S. Ahn, Allen J. Bard

Center for Electrochemistry, Department of Chemistry, The University of Texas at Austin, Austin, Texas 78712, United States

ajbard@mail.utexas.edu

Contents:

Experimental procedures

Materials. $Bi(NO_3)_3 \cdot 5H_2O$ (99.999%) , VCl_3 (99%), $(NH_4)_{10}W_{12}O_{41} \cdot 5H_2O$ (99.999%) were purchased from Alfa-Aesar (Ward Hill, MA, USA). Ferrocenemethanol (FcMeOH, 97%) and $TiCl_3$ (12% Ti in HCl solution) were purchased from Sigma-Aldrich (St. Louis, MO, USA). $Co(CH_3COO_2) \cdot 4H_2O$ (>98%, Acros Organics), NaH_2PO_4 (99.5%), Na_2HPO_4 (99.9%), Na_2SO_3 (99.4%), ethanol, acetone and ethylene glycol were purchased from Fisher Scientific (Pittsburgh, PA, USA). All chemicals were used as received. Solutions were prepared with Milli-Q deionized water (18 MΩ). Fluorine doped tin oxide coated glass (FTO, <14 Ω, Pilkington, Toledo, OH) was cleaned by ultrasonication in ethanol and used as a substrate for the thin films.

Preparation of photoelectrodes. Precursor solutions of VCl_3, $Bi(NO_3)_3 \cdot 5H_2O$, and $(NH_4)_{10}W_{12}O_{41} \cdot 5H_2O$ (20 mM in ethylene glycol) were mixed at a volume ratio of 50:45:5, respectively. The solution was drop-cast (300 μL) on a FTO substrate (15mm×25 mm) immediately after the substrate was heated to 200°C/1hr and cooled to room temperature. The samples were then dried in air (110°C / 2 hrs) and annealed in air (500°C / 3 hrs, heat rate 1°C/min), affording yellow films. Before measurement, some weakly bound powder was removed by scotch tape, followed by acetone and water rinsing. Co_3O_4 nanoparticles were synthesized according to a literature procedure;[1] briefly, 170 mg $Co(CH_3COO_2) \cdot 4H_2O$ were added to a mixture of 2.3 mL H_2O, 5.0 mL ethanol, and 0.83 mL NH_4OH, stirred, and heated in a Teflon-lined autoclave at 150°C overnight, to yield 11 nm particles. Following several cycles of washing in ethanol, the particle dispersion was diluted x10, deposited at 0.015 mg/cm^2 (as determined by weighing known-area samples), and dried for 10 minutes.

Photoelectrochemistry. The active area of the W:$BiVO_4$/FTO electrode was defined by a Viton O-ring (inner A = 0.38 cm^2), which was pressed to a window in the borosilicate cell. The sample was illuminated from the front, at a light intensity of 40 mW/cm^2 at 500 nm. Unless stated otherwise, a Pt coil counter electrode and a Ag/AgCl reference electrode (in 1 M KCl, CH Instruments) were used to complete the 3-electrode setup. Potentials are reported with respect to the reversible hydrogen electrode (RHE, –0.235 V vs. Ag/AgCl/KCl-1M at room temperature).

Electrodeposition of a-TiO_2.

The electrodeposition of *a*-TiO_2 was performed as described in the literature with moderate modifications.[2,3] $TiCl_3$ solution for the electrodeposition of *a*-TiO_2 was prepared by diluting 12% $TiCl_3$ solution in HCl 1:20 in deionized water (total volume 21 mL), followed by neutralization of the pH of the solution to 2.45 ± 0.03 by slow addition of 0.6 M $NaHCO_3$ solution. The pH adjustment was accompanied by color change of the solution from reddish purple to deep purple, and the added volume of the solution led to a final Ti concentration of

ca. 15 mM. The electrodeposition process was performed by applying 0.02 V vs. SCE (CH Instruments) onto a W:$BiVO_4$ coated FTO working electrode immersed in a $TiCl_3$ deposition solution. Deposition progress was monitored by chronoamperometry (Figure S1). The deposition times were varied as a control for film thickness (see manuscript). Note that the pH control in the electrodeposition of *a*-TiO_2 is critical because much different outcome can be expected from solutions differing in acidity by 0.5 pH units. Solutions were freshly made prior to deposition, and no solution older than 2 hr was used. After deposition, care was taken to avoid current spikes at the working electrode, since they occasionally damage the *a*-TiO_2 film.

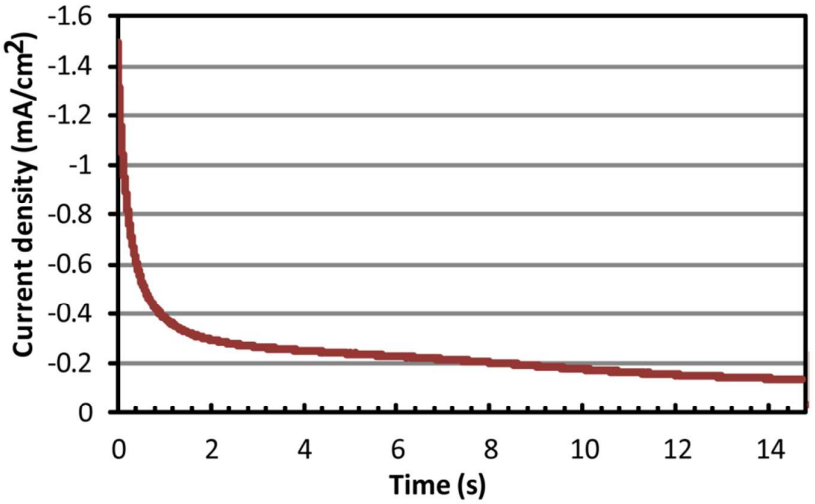

Figure S1. Chronoamperometry of *a*-TiO_2 electrodeposition on W:$BiVO_4$/FTO, from 15 mM $TiCl_3$ solution at pH = 2.45. The charge transferred to solution was –3.5 mC/cm^2.

Instruments. All electrochemical measurements were performed on a CH Instruments (Austin, TX, USA) model 630D potentiostat. A Xe lamp (XBO 150 W, Osram, Munich, Germany) was used for illumination. A silicon photodetector (818-UV, Newport, Irvine, CA, USA) with an attenuator (OD3, Newport) and an optical power meter (1830-C, Newport) were used to calibrate the light intensity. W:$BiVO_4$ samples were characterized by scanning electron microscopy (Quanta 650 FEG, FEI Company, Inc., Hillsboro, OR, USA) following sputtering of a Pd:Au layer, deposited to minimize sample charging. The *a*-TiO_2 layer was characterized by X-ray photoelectron spectroscopy (Kratos XPS, Kratos Analytical Ltd., UK) equipped with a monochromatic Al X-ray source. Glancing incidence angle X-ray diffraction measurements were performed by using D8 ADVANCE (Bruker, Fitchburg, WI, USA) equipped with a Cu Kα radiation source where the incident angle was 0.4°. Diffuse reflectance UV−vis spectra were measured with a Cary 500 spectrophotometer attached to an integrating sphere (Labsphere DRA-CA-5500).

X-ray diffraction and photoelectron spectroscopy of *a*-TiO_2 on W:$BiVO_4$/FTO

Glancing angle X-ray diffraction (XRD) of *a*-TiO_2/W:$BiVO_4$/FTO revealed the characteristic diffraction peaks for $BiVO_4$ (clinobisvanite, syn, 00-014-0688) and SnO_2 (00-046-1088), but none of the known patterns of TiO_2 (Figure S2).

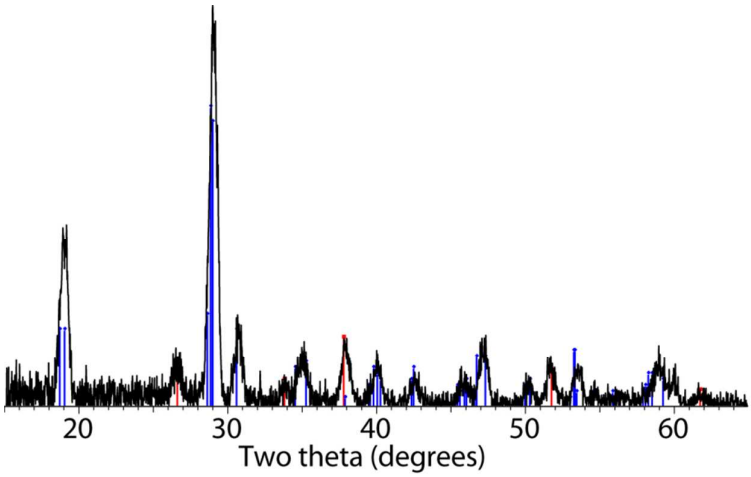

Figure S2. XRD spectrum of an *a*-TiO_2 film on a W:$BiVO_4$ (blue) / FTO (red) electrode.

The binding energy peaks of 458.9 eV and 464.7 eV (Figure S3) correspond to $2p_{3/2}$ and $2p_{1/2}$ orbitals of Ti(IV) in TiO_2.[19] This indicates that the electrodeposited film is largely TiO_2, similar to TiO_2 films prepared by this method previously.

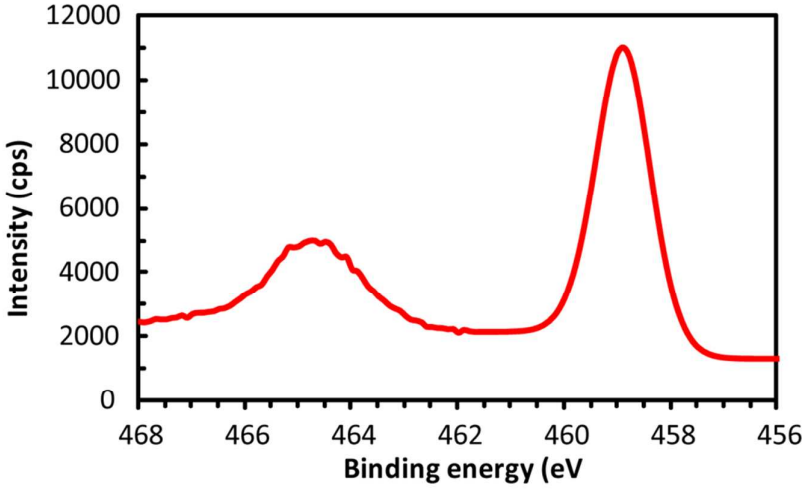

Figure S3. XPS spectrum of an electrodeposited *a*-TiO_2 film on a W:$BiVO_4$/FTO electrode, in the Ti 2p core energy region.

Stability of photocurrent on *a*-TiO_2-coated W:$BiVO_4$/FTO

Figure S4 presents the photocurrent on two W:$BiVO_4$/FTO electrodes held overnight at a potential of 0.83 V vs. RHE and under unfiltered xenon lamp illumination. Following an initial decrease, typical to $BiVO_4$ photoanodes,[4,13,14] the improved current is stable for over 12 hours. The irregularities in the current correspond to the formation and release of oxygen bubbles (as observed by naked eye). Clearly, the enhancement in photocurrent obtained from the *a*-TiO_2 coating does not diminish over time.

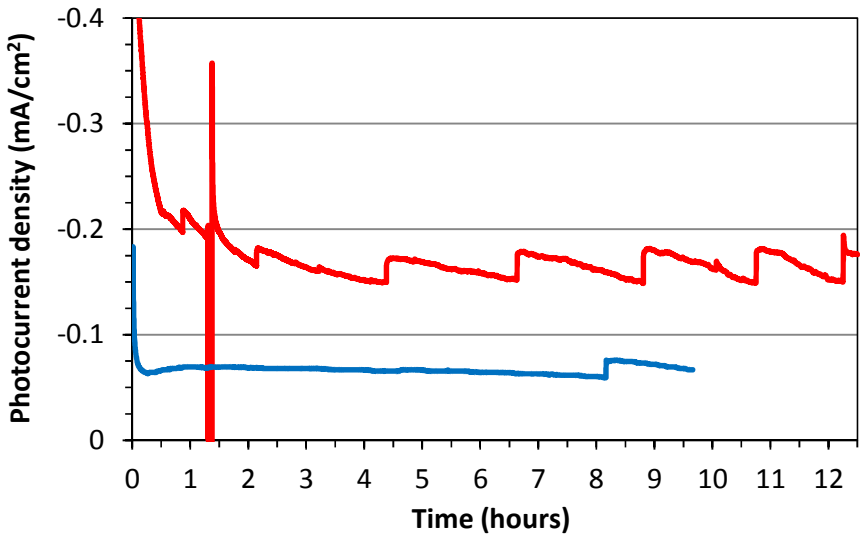

Figure S4. Chronoamperometry of W:$BiVO_4$/FTO electrodes, with (red trace) and without (blue trace, stopped after 9.5 hours) a coating of amorphous TiO_2.

Variability in FTO reactivity on W:$BiVO_4$/FTO electrodes

The reactivity of the exposed FTO regions on W:$BiVO_4$/FTO was tested by oxidation of FcMeOH in the dark (Figure S5). It was found to vary significantly between samples, owing both to variations in spacing between W:$BiVO_4$ grains (which affect the rate of growth and coalescence of the diffusion layer), as well as to the inherent irregularities in FTO reactivity, which has been reported in the literature.[20,21] Washing the samples by organic solvents (ethanol, acetone, isopropanol) did not affect the reactivity.

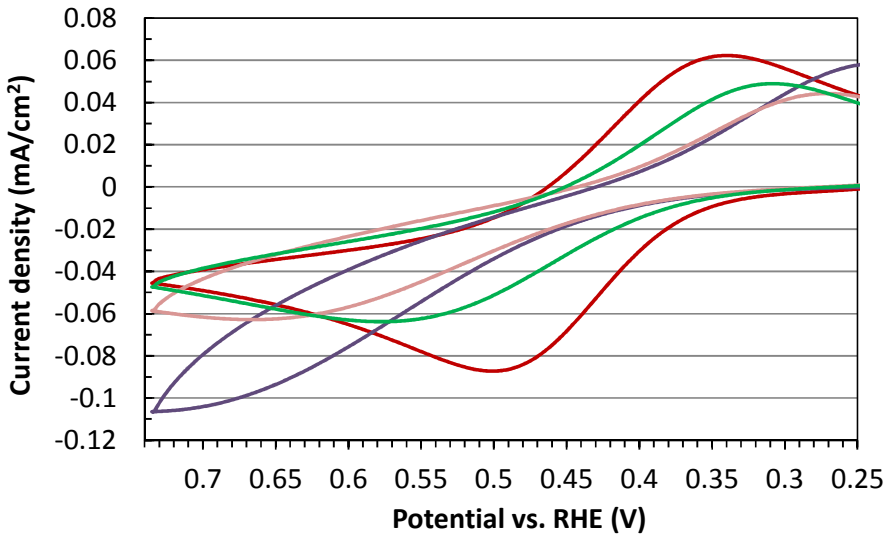

Figure S5. Cyclic voltammetry of FcMeOH (1 mM in 0.1 M, pH 7.0 phosphate buffer) on several W:$BiVO_4$/FTO electrodes, in the dark, demonstrating the inherent variability in electrochemical reactivity of the exposed FTO regions.

Scanning electron micrographs of *a*-TiO_2/W:$BiVO_4$

Since the reactivity of FTO varies between samples, and even between different regions of the same sample (see above), regions of thinner or thicker *a*-TiO_2 films can be found even on samples with optimal (15–30 s) deposition times. Scanning electron micrographs (SEM) of lower coverage regions give an idea of the growth process (Figure S7). The *a*-TiO_2 is the amorphous matter connecting W:$BiVO_4$ particles; it appears mostly between the particles and at their sides, and so seems to creep on them the FTO (on which it must initiate due to the inability of *n*-W:$BiVO_4$ to support an oxidizing current).

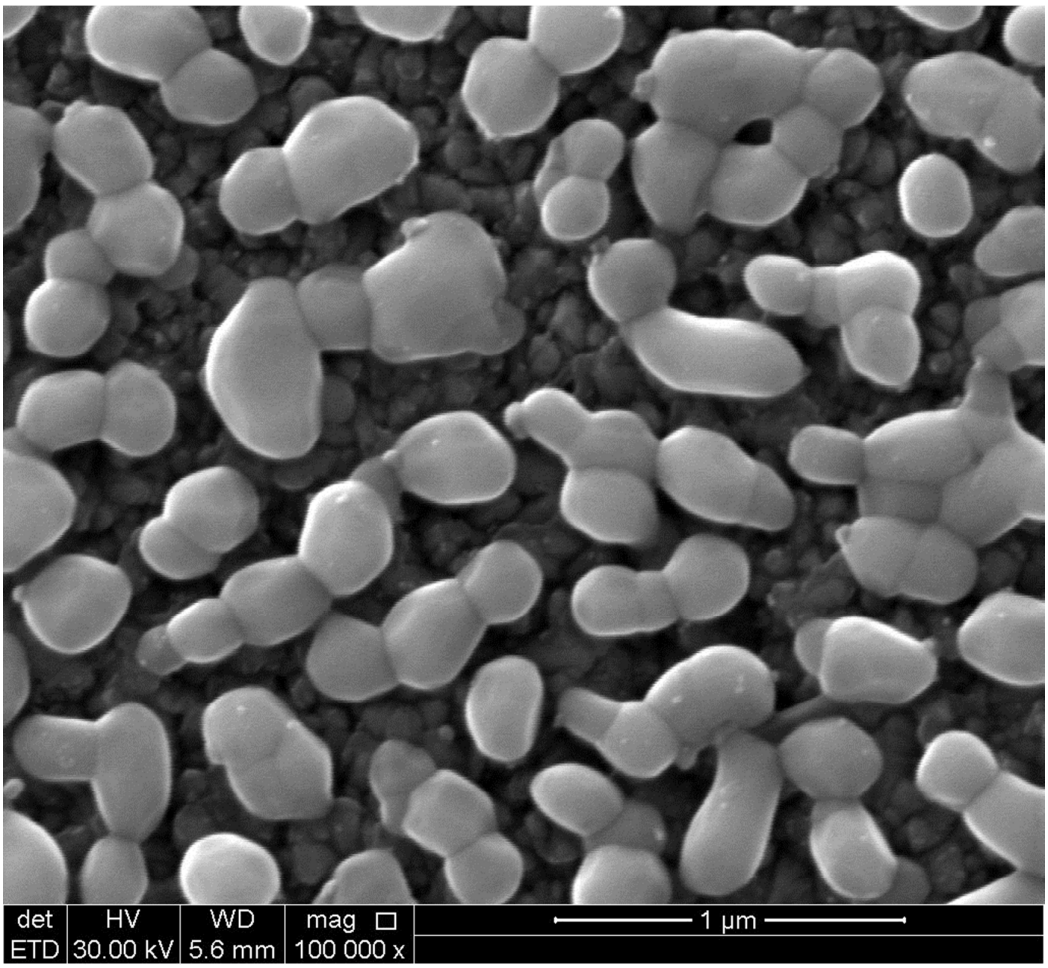

Figure S6. SEM of a W:$BiVO_4$/FTO electrode, before *a*-TiO_2 deposition.

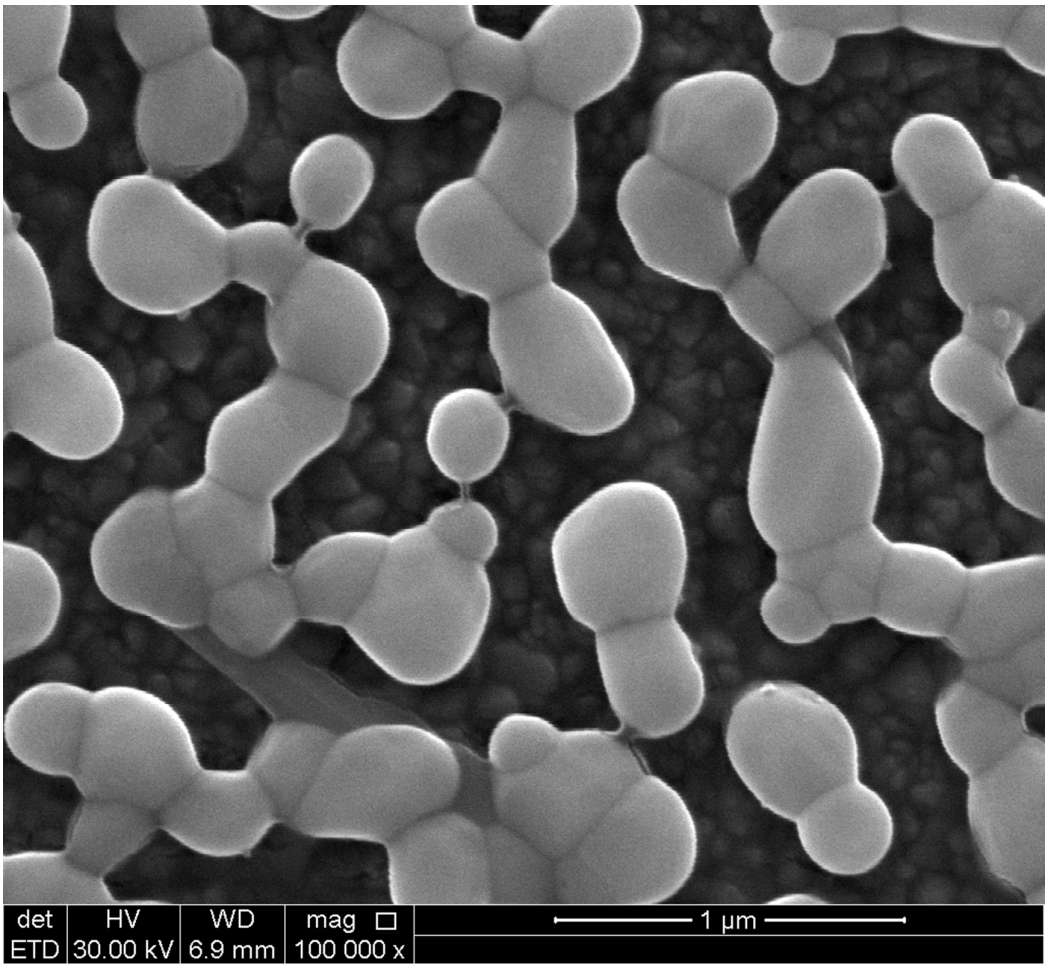

Figure S7. SEM of a low coverage region of *a*-TiO_2/W:$BiVO_4$/FTO electrode.

Effect of deposition time variation on water oxidation photocurrent

a-TiO_2 films electrodeposited for very short times (<5 seconds, Figure S8) or very long (>50 seconds, Figure S9) do not enhance the water oxidation photocurrent – in contrast to the optimal, 15–30 s depositions (Figure 2 in the manuscript).

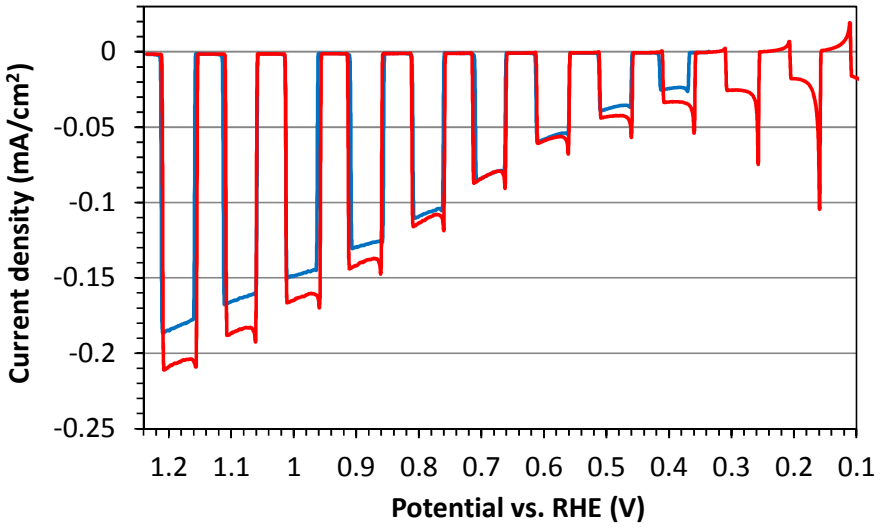

Figure S8. Linear scan voltammetry of W:$BiVO_4$/FTO in 0.1 M, pH = 7.0 phosphate buffer, under chopped illumination, before (blue trace) and after (red trace) electrodeposition of *a*-TiO_2 for 5 seconds. Scan rate is 25 mV/s.

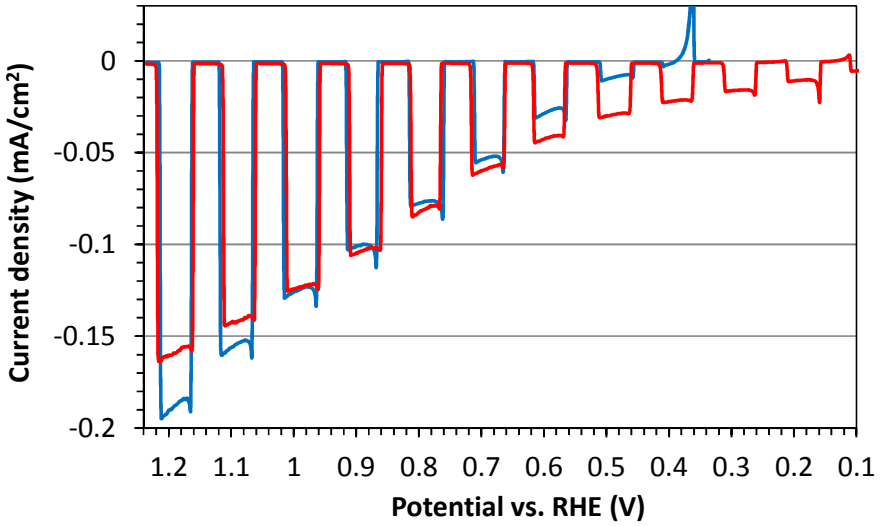

Figure S9. Linear scan voltammetry of W:$BiVO_4$/FTO in 0.1 M, pH = 7.0 phosphate buffer, under chopped illumination, before (blue trace) and after (red trace) electrodeposition of *a*-TiO_2 for 5 minutes. Scan rate is 25 mV/s. Deposition durations of 50 seconds and above afford similar results.

Electrochemistry on *a*-TiO_2/FTO

Amorphous TiO_2 films were electrodeposited directly on FTO samples, to test for electro- and photo-catalytic effects in the absence of W:$BiVO_4$. The deposition procedure was identical to that on W:$BiVO_4$/FTO electrodes, and deposition times ranged between 15 and 30 seconds. The *a*-TiO_2 film in itself showed no photo-response whatsoever (FcMeOH oxidation, Figure S11), and no catalytic effect for water oxidation (Figure S10). For comparison to a real catalytic effect, Co_3O_4 nanoparticles were deposited on the *a*-TiO_2/FTO electrode, giving rise to a dramatic enhancement of water oxidation current (Figure S10, green trace).

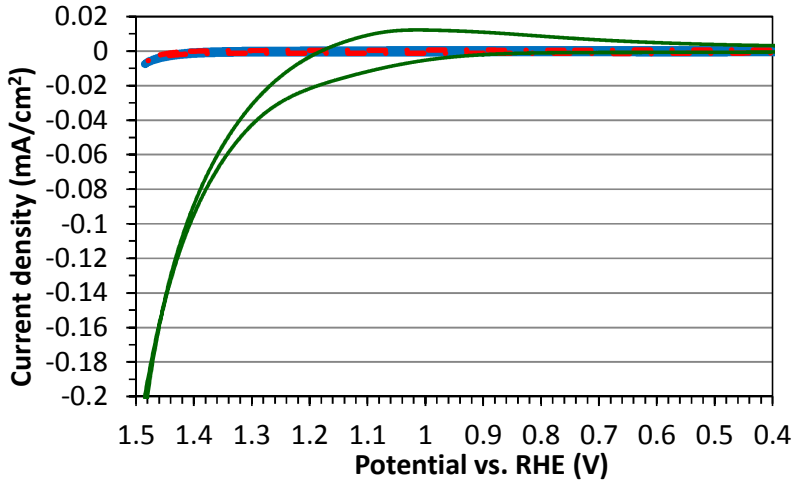

Figure S10. Cyclic voltammetry in 0.1 M, pH 7.0 phosphate buffer, before (blue trace) and after (red dashed trace) *a*-TiO_2 electrodeposition on FTO (15 s). The *a*-TiO_2 film shows no electrocatalytic activity towards water oxidation. Addition of Co_3O_4 nanoparticles (0.015 mg/cm^2) demonstrates the effect of a true catalytic layer (green trace).

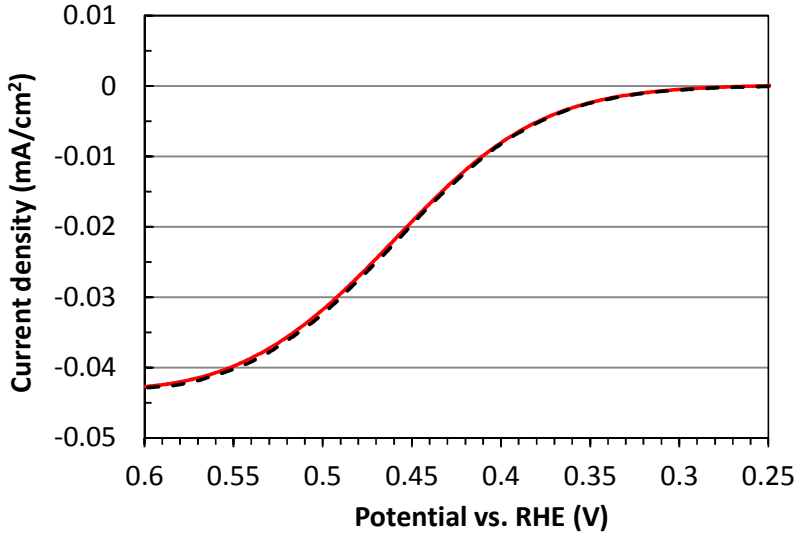

Figure S11. Linear scan voltammetry of FcMeOH (1 mM in 0.1 M, pH 7.0 phosphate buffer) on a *a*-TiO_2/FTO electrode, in the dark (red trace) and under chopped illumination (black dashed trace). The electrodeposited *a*-TiO_2 film shows no photocatalytic activity.

UV-vis spectroscopy of W:$BiVO_4$/FTO

A UV-vis spectrum of W:$BiVO_4$/FTO was collected in an integrating sphere spectrometer, before and after a 15 seconds-long electrodeposition of *a*-TiO_2 (Figure S12). The minor improvement in absorption (more pronounced in the UV region), cannot account for the observed dramatic improvement in photocurrent.

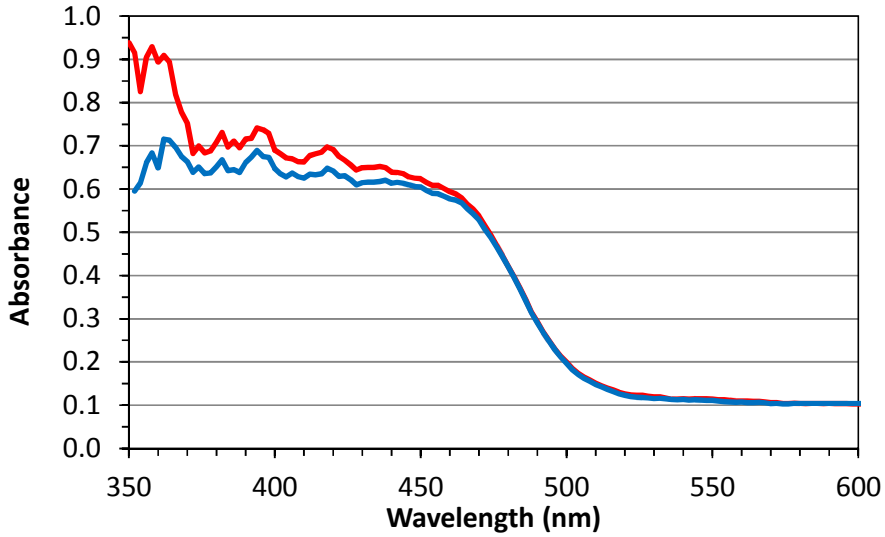

Figure S12. UV-vis spectrum of a W:$BiVO_4$/FTO electrode, before (blue trace) and after (red trace) a 15 seconds-long electrodeposition of *a*-TiO_2.

Incident photon-to-current efficiency

To obtain the incident photon-to-current efficiency (IPCE) spectrum (Figure S13), the photocurrent was measured at 0.83 V vs. RHE under monochromatic radiation, by alternating illumination (2–3 seconds) with darkness (7–8 seconds) during a chronoamperometric experiment. The net photocurrent at each wavelength was extracted by subtracting the background current. The IPCE, which expresses the ratio of extracted photogenerated power to the incident irradiation power, was calculated at each wavelength using the equation:

$$\text{IPCE (\%)} = i_{ph} / (P_{in} \cdot \lambda / 1240) \cdot 100\%$$

Where i_{ph} is the measured photocurrent in mA, P_{in} is the incident power in mW, and λ is the wavelength of incident light in nm.

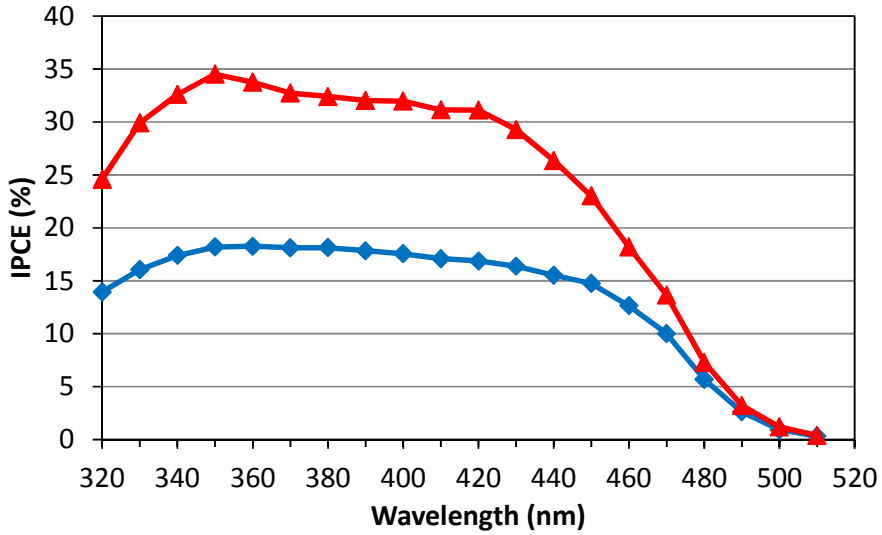

Figure S13. IPCE of a W:$BiVO_4$/FTO electrode in 0.1 M, pH = 7.0 phosphate buffer, before (blue trace) and after (red trace) electrodeposition of *a*-TiO_2 for 15 seconds.

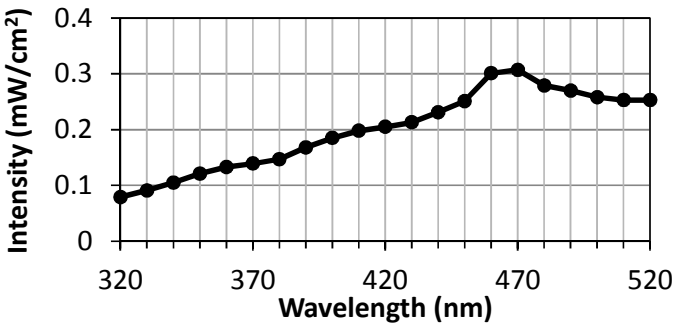

Figure S14. Light intensity through the monochromator during IPCE measurement.

Effect of co-catalyst: Co_3O_4 nanoparticles

An additional layer of Co_3O_4 nanoparticles, deposited by drop-casting on a *a*-TiO_2-covered W:$BiVO_4$/FTO electrode, further improves the water oxidation photocurrent (Figure S15). However, the enhancement due *a*-TiO_2 electrodeposition alone, already constitutes a major part (75% at 0.82 V vs. RHE) of the overall improvement, even though the *a*-TiO_2 film is not catalytic.

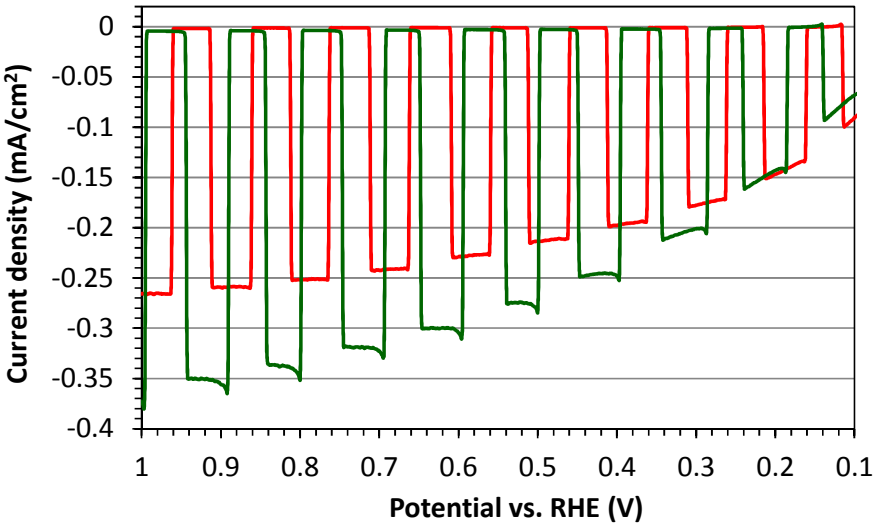

Figure S15. Linear scan voltammetry of W:$BiVO_4$/FTO in 0.1 M, pH = 7.0 phosphate buffer, under chopped illumination, after electrodeposition of *a*-TiO_2 (15 s, red trace) and after both *a*-TiO_2 and Co_3O_4 deposition. Scan rate is 25 mV/s.

References

(1) Dong, Y.; He, K.; Yin, L.; Zhang, A. *Nanotechnology* **2007**, *18*, 435602.
(2) Kavan, L.; Stoto, T.; Grätzel, M.; Fitzmaurice, D.; Shklover, V. *J. Phys. Chem.* **1993**, *97*, 9493.
(3) Kavan, L.; O'Regan, B.; Kay, A.; Grätzel, M. *J. Electroanal. Chem.* **1993**, *346*, 291.
(4) Zhong, D. K.; Choi, S.; Gamelin, D. R. *J. Am. Chem. Soc.* **2011**, *133*, 18370.
(5) Liang, Y.; Tsubota, T.; Mooij, L. P. A.; van de Krol, R. *J. Phys. Chem. C* **2011**, *115*, 17594.
(6) Berglund, S. P.; Rettie, A. J. E.; Hoang, S.; Mullins, C. B. *Phys. Chem. Chem. Phys.* **2012**, *14*, 7065.
(7) Choi, S. K.; Choi, W.; Park, H. *Phys. Chem. Chem. Phys.* **2013**, *15*, 6499.
(8) Ding, C.; Shi, J.; Wang, D.; Wang, Z.; Wang, N.; Liu, G.; Xiong, F.; Li, C. *Phys. Chem. Chem. Phys.* **2013**, *15*, 4589.
(9) Stoughton, S.; Showak, M.; Mao, Q.; Koirala, P.; Hillsberry, D. A.; Sallis, S.; Kourkoutis, L. F.; Nguyen, K.; Piper, L. F. J.; Tenne, D. A.; Podraza, N. J.; Muller, D. A.; Adamo, C.; Schlom, D. G. *Apl Mater.* **2013**, *1*, 042112.
(10) Seabold, J. A.; Zhu, K.; Neale, N. R. *Phys. Chem. Chem. Phys.* **2014**, *16*, 1121.
(11) Alarcón-Lladó, E.; Chen, L.; Hettick, M.; Mashouf, N.; Lin, Y.; Javey, A.; Ager, J. W. *Phys. Chem. Chem. Phys.* **2014**, *16*, 1651.
(12) Sayama, K.; Nomura, A.; Zou, Z.; Abe, R.; Abe, Y.; Arakawa, H. *Chem. Commun.* **2003**, 2908.
(13) Sayama, K.; Nomura, A.; Arai, T.; Sugita, T.; Abe, R.; Yanagida, M.; Oi, T.; Iwasaki, Y.; Abe, Y.; Sugihara, H. *J. Phys. Chem. B* **2006**, *110*, 11352.
(14) Jia, Q.; Iwashina, K.; Kudo, A. *Proc. Natl. Acad. Sci.* **2012**, *109*, 11564.
(15) Wang, D.; Li, R.; Zhu, J.; Shi, J.; Han, J.; Zong, X.; Li, C. *J. Phys. Chem. C* **2012**, *116*, 5082.
(16) Jeong, H. W.; Jeon, T. H.; Jang, J. S.; Choi, W.; Park, H. *J. Phys. Chem. C* **2013**, *117*, 9104.
(17) Wang, G.; Ling, Y.; Lu, X.; Qian, F.; Tong, Y.; Zhang, J. Z.; Lordi, V.; Rocha Leao, C.; Li, Y. *J. Phys. Chem. C* **2013**, *117*, 10957.
(18) Chen, L.; Alarcón-Lladó, E.; Hettick, M.; Sharp, I. D.; Lin, Y.; Javey, A.; Ager, J. W. *J. Phys. Chem. C* **2013**, *117*, 21635.
(19) Kim, J.; Kim, B.-K.; Cho, S. K.; Bard, A. J. *J. Am. Chem. Soc.* **2014**, *136*, 8173.
(20) Cameron, P. J.; Peter, L. M.; Hore, S. *J. Phys. Chem. B* **2005**, *109*, 930.
(21) Ofir, A.; Grinis, L.; Zaban, A. *J. Phys. Chem. C* **2008**, *112*, 2779.